Analysis of sharp-tip-indentation load–depth curve for contact area determination taking into account pile-up and sink-in effects

Yeol Choi[a], Ho-Seung Lee, and Dongil Kwon
School of Materials Science and Engineering, Seoul National University, Seoul 151-742, Korea

(Received 27 April 2004; accepted 2 August 2004)

Hardness and elastic modulus of micromaterials can be evaluated by analyzing instrumented sharp-tip-indentation load–depth curves. The present study quantified the effects of tip-blunting and pile-up or sink-in on the contact area by analyzing indentation curves. Finite-element simulation and theoretical modeling were used to describe the detailed contact morphologies. The ratio f of contact depth, i.e., the depth including elastic deflection and pile-up and sink-in, to maximum indentation depth, i.e., the depth measured only by depth sensing, ignoring elastic deflection and pile-up and sink-in, was proposed as a key indentation parameter in evaluating real contact depth during indentation. This ratio can be determined strictly in terms of indentation-curve parameters, such as loading and unloading slopes at maximum depth and the ratio of elastic indentation energy to total indentation energy. In addition, the value of f was found to be independent of indentation depth, and furthermore the real contact area can be determined and hardness and elastic modulus can be evaluated from f. This curve-analysis method was verified in finite-element simulations and nanoindentation experiments.

I. INTRODUCTION

The nanoindentation technique, which can measure the applied indentation loads of the micro-Newton to milli-Newton scale and very shallow indentation depths of nanometer scale, has been widely used to evaluate mechanical properties of small-volume materials such as thin films, coating layers, and multiphase materials.[1–3] In particular, it can obviate the many practical difficulties arising in direct measurement of a residual contact impression at nanometer scales. With this technique, the equipment records load and depth continuously and all the results, mainly hardness and elastic modulus, are evaluated only by analysis of an indentation load–depth curve. Since the contact area is calculated from contact depth using the geometrical relation of the indenter, it is important to be able to determine contact depth accurately from the indentation load–depth curve.

As a typical indentation curve analysis, Oliver and Pharr suggest that contact depth be determined by subtracting the elastic deflection depth at the contact perimeter from the maximum indentation depth through analysis of the indentation unloading curve [Figs. 1(a) and 1(b)].[4] This method has widely been adopted in the instrumented indentation field and has also been extended and refined.[5–9]

There is, however, practical difficulty in this method for obtaining mechanical properties at small scales. It cannot take into account pile-up around the contact impression. Figure 2 shows the contact morphologies with pile-up. As pile-up occurs, the real contact area increases more than the calculated area (which takes into account only elastic deflection under a reference plane[4]).[7–11] Its underestimation of contact area yields the overestimation of the hardness and elastic modulus of ductile materials. Accordingly, a few researches were suggested to consider pile-up effect in contact area determination from indentation L-h curve, but they had some difficulties to be used practically because they needed pre-known mechanical properties or pre-testing information from large-scale indentations, in which the residual indentations with pile-up or sink-in was easy to be observed.[7–10]

On the other hand, the indenter tip such as Berkovich and conical indenter is not perfectly sharp due to manufacturing limitations and wear.[4,11–13] If this tip blunting is not considered in contact depth determination from the L-h curve, the curve analysis results also underestimate the contact area because the area calculation assumes a perfectly sharp indenter in instrumented indentation.

This study introduces a new indentation-curve analysis method that quantitatively includes both pile-up/sink-in

[a]Address all correspondence to this author.
e-mail: yariman@snu.ac.kr or ychoi@frontics.com
DOI: 10.1557/JMR.2004.0419

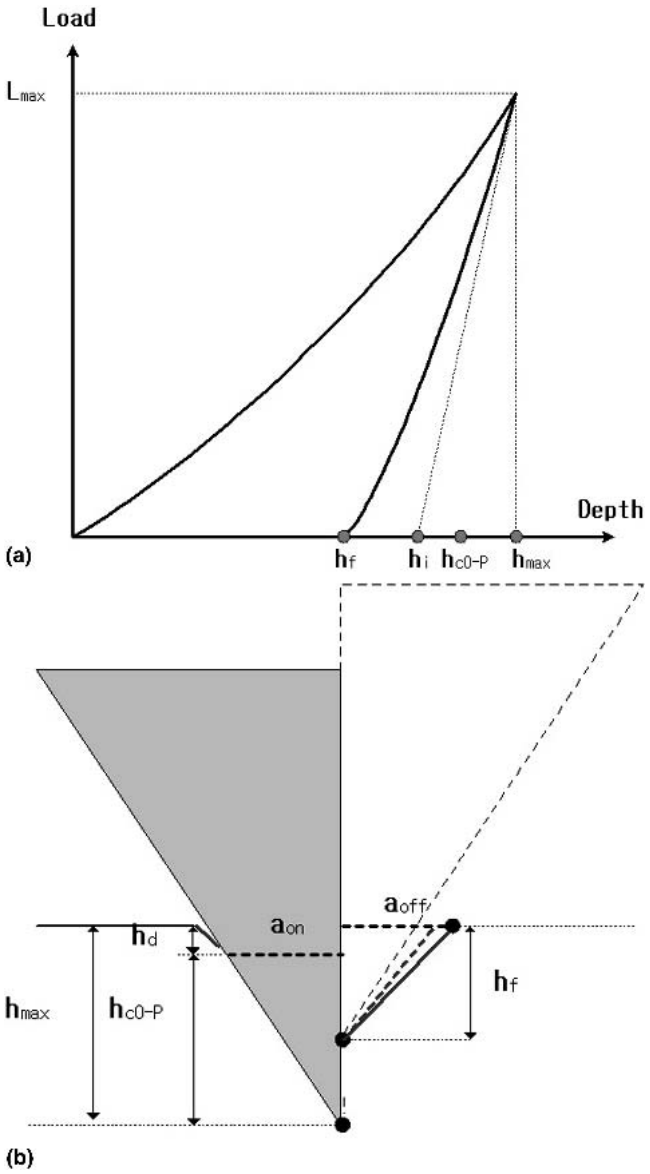

FIG. 1. Schematic diagrams of (a) typical indentation load–depth curve and (b) indentation contact morphology during maximum loading, without pile-up and sink-in effects.

and tip blunting. The real contact morphology, including pile-up or sink-in around the contact impression and the tip-blunting effects, is defined, and equations for determining the contact depth only from curve parameters are suggested on the basis of the contact morphology. The new method was verified by finite-element analysis (FEA) and experiments with nanoindentations.

II. INDENTATION CURVE ANALYSIS BASED ON CONTACT MORPHOLOGY

Figure 1(a) shows a typical indentation load–depth curve. Oliver and Pharr suggested that contact depth

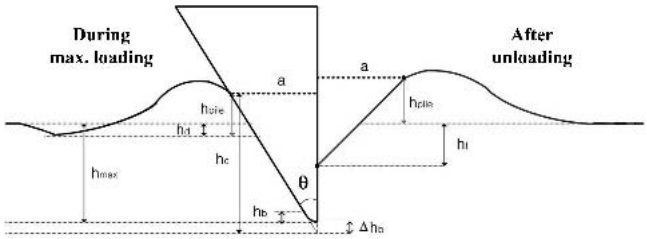

FIG. 2. Schematic diagram of real contact morphologies with large pile-up around indent and tip-blunting.

$h_{c(op)}$ could be expressed in terms of maximum indentation depth h_{max} and elastic deflection at the contact perimeter h_d,[4] where ϵ is a constant dependent on indenter geometry

$$h_c = h_{max} - h_d = h_{max} - \epsilon(h_{max} - h_i) \quad . \tag{1}$$

Also, contact area is determined using indenter geometry if a conical indenter with half-included angle θ is assumed

$$A_c = \pi(\tan^2 \theta)h_c^2 \quad . \tag{2}$$

For the Berkovich, Vickers and conical indenters with $\theta = 70.3°$, the contact area can be expressed as $24.56h_c^2$.

The above analysis, based on the simple contact morphology in Fig. 1(b), does not take into account pile-up and tip-blunting effects. A modified contact morphology for the conical indentation at maximum loading, assumed to be as in Fig. 2, includes the pile-up depth h_{pile} and a correction depth for tip blunting Δh_b. From this contact morphology, the contact depth and area can be redefined as in Eqs. (3) and (4). The contact depth (h_c) is determined by considering the elastic deflection depth (h_d), plastic pile-up depth (h_{pile}), and the correction depth for tip blunting (Δh_b) in addition to the maximum indentation depth from the reference plane (h_{max})

$$h_c = h_{max} + h_{pile} - h_d + \Delta h_b \quad , \tag{3}$$

$$A_c = \pi \tan^2 \theta \, (h_{max} + h_{pile} - h_d + \Delta h_b)^2 \quad . \tag{4}$$

At that time, remember that the tip-blunting effect consideration in Eq. (4) is available only for much deeper indentation than the blunted depth, h_b if an indenter was blunted at the tip.

The ratio f of contact depth h_c to the sum of maximum depth h_{max} and the correction depth for tip blunting Δh_b can be defined as in Eq. (5); it can also be taken as constant if the material is homogeneous and the indenter geometry is self-similar.[10]

$$f = \frac{h_c}{h_{max} + \Delta h_b} = \frac{h_{max} + h_{pile} - h_d + \Delta h_b}{h_{max} + \Delta h_b} \quad . \tag{5}$$

Then contact area can be determined in terms of f, h_{max}, and Δh_b as in Eq. (6)

$$A_c = \pi(\tan^2 \theta)f^2(h_{max} + \Delta h_b)^2 \quad . \tag{6}$$

Indentation hardness is defined in terms of maximum load and contact area

$$H = \frac{L_{\max}}{A_c} \quad . \tag{7}$$

Substituting Eqs. (5) and (6) into Eq. (7) and rearranging yields the expression for the indentation loading curve in Eq. (8), which agrees with other works in showing indentation load proportional to the square of the depth during loading.[12–15]

$$L = \pi(\tan^2\theta)Hf^2(h + \Delta h_b)^2 = K_1(h + \Delta h_b)^2 \quad . \tag{8}$$

Accordingly, the blunting depth Δh_b can be obtained from the slope and the x axis intercept value in a linear fitting of the square root of load and depth.

On the other hand, the unloading curve can be expressed as Eq. (9)[4]

$$L = K_2(h - h_f)^m \quad . \tag{9}$$

The slopes of the loading and unloading curves at maximum load, S_L and S_U, respectively, are determined by differentiating Eqs. (8) and (9) at maximum load[4]

$$S_U = K_2 m(h_{\max} - h_f)^{m-1} = \beta \frac{2}{\sqrt{\pi}} E_r \sqrt{A_c} \quad , \tag{10}$$

$$S_L = 2K_1(h_{\max} + \Delta h_b) = 2\pi(\tan^2\theta)Hf^2(h_{\max} + \Delta h_b) \quad . \tag{11}$$

β is a correction factor for the deviation from axisymmetry of the indenter and radial displacement based on Sneddon's equation and E_r is the reduced elastic modulus.[5,9,16] Then, combining Eqs. (6), (10), and (11) lets us describe f as the ratio of the slopes (S_L/S_U) and E_r/H_r

$$f = \left(\frac{\beta}{\pi \tan\theta}\right)\left(\frac{S_L}{S_U}\right)\left(\frac{E_r}{H}\right) \quad . \tag{12}$$

To evaluate the depth ratio f using only the indentation loading and unloading curves, E_r/H must be expressed by indentation parameters. The ratio of elastic energy to total energy is introduced as a parameter related to E_r/H. Elastic indentation energy and total indentation energy are determined from integration of the unloading and loading curves, respectively, as shown in Eqs. (13) and (14). This energy ratio can be expressed as Eq. (15)

$$W_e = \int_{h_f}^{h_{\max}} K_2(h - h_f)^m \, dh = \frac{1}{m+1} K_2(h_{\max} - h_f)^{m+1} \quad , \tag{13}$$

$$W_{tot} = \int_0^{h_{\max}} K_1(h + \Delta h_b)^2 \, dh \approx \frac{1}{3} K_1(h_{\max} + \Delta h_b)^3 \quad , \tag{14}$$

$$\frac{W_e}{W_{tot}} = \frac{3}{m+1}\left(\frac{h_{\max} - h_f}{h_{\max} + \Delta h_b}\right) \quad . \tag{15}$$

This energy ratio has been found to have a linear relation to the ratio of hardness to elastic modulus in Eq. (16), where κ is a proportional constant with value about 5 independent of materials for a conical indenter with half-included angle of 70.3° or Berkovich indenter.[9,17–22]

$$\frac{W_e}{W_{tot}} = \kappa \frac{H}{E_r} \quad . \tag{16}$$

Thus, the value of f can be obtained from only the indentation load–depth curve in Eq. (17) by employing Eqs. (12), (15), and (16)

$$f = \frac{\beta\kappa(m+1)}{3\pi \tan\theta}\left(\frac{S_L}{S_u}\right)\left(\frac{h_{\max} + \Delta h_b}{h_{\max} - h_f}\right) \quad . \tag{17}$$

Also, hardness and elastic modulus can be evaluated by substituting the contact area obtained from the f value into Eqs. (7) and (10), respectively.

III. EXPERIMENTS AND SIMULATION PROCEDURES

A. Finite-element simulation

An axisymmetric two-dimensional finite-element model was constructed to simulate the indentation response of elastoplastic materials with various sets of yield strength σ_{ys}, elastic modulus E, Poisson's ratio ν, and work-hardening exponent n, using the commercial software ABAQUS (Hibbitt, Karlsson and Sorensen, Inc., Pawtucket, RI). The materials properties used in the simulation are shown in Table I. A total of 3722 four-node bilinear axisymmetric quadrilateral elements were used. A fine mesh near the contact region becoming gradually coarser further from the contact region was designed to ensure numerical accuracy (Fig. 3). A semi-cone angle of 70.3° was chosen for the ideally sharp-tip indenter to give the same area at any depth with the

TABLE I. Mechanical properties of materials used in FEA.

E (GPa)	σ_{ys} (MPa)	n	ν
217	568	0.113	0.272
210	598	0.178	0.282
74	269	0.187	0.341
207	336	0.221	0.295
219	345	0.225	0.286
212	285	0.232	0.284
411	310	0.450	0.280
70	2662	0	0.250
90	3000	0.300	0.300
200	2000	0.350	0.170
100	3000	0.350	0.170
70	3500	0.300	0.17
70	2000	0.250	0.17
70	3000	0.200	0.17

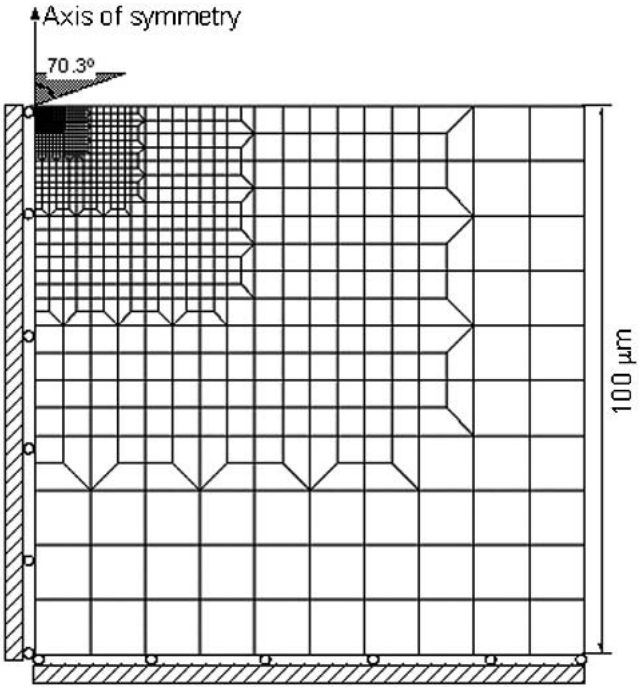

FIG. 3. Axisymmetric mesh used in finite-element simulations.

Berkovich pyramid. Indentations using a blunted sharp-tip indenter with tip radius of 450 nm and Δh_b of 28 nm in 70.3° semi-cone angle were also simulated. The indenter was modeled as a rigid body.

A downward displacement was imposed on the indenter, causing it to be pushed into the surface of the material to 250-nm maximum depth to simulate the indentation process. The loading and unloading curves were obtained directly from the ABAQUS output of the total reaction force in the normal direction on the rigid indenter as a function of indenter vertical displacement. Contact information such as h_c, h_{pile}, and h_d was observed and determined from contact profiles during and after loading.

B. Nanoindentations

Nanoindentations were made on glass, fused quartz, pure Cu and Au film of 1.3 μm thickness on a Si substrate using a Berkovich indenter. Indentation loads from 3,000 to 16,000 μN in the case of fused quartz, and from 200 to 10,000 μN in the case of pure Cu, were applied to verify the dependencies of f, H, and E on indentation depth. In cases of Au film and glass, 2,000 and 10,000 μN, respectively, was applied as a maximum indentation load. Loading rate was 100 μN/s, and multiple unloadings were made to minimize time-dependent deformation effects. The machine compliance was determined and corrected for accurate load–depth curves. After indenting, residual impressions were observed with an atomic force microscope (AFM), and real contact area was calculated by an image analyzer.

IV. RESULTS AND DISCUSSION

A. Loading-curve analysis considering tip-blunting effect

Loading curves with and without tip blunting are fitted as the square root of indentation load versus indentation depth to verify the loading-curve derivation in Eq. (8) (Fig. 4). This perfect linear relationship means that the indentation load is proportional to the square of indentation depth. It should be emphasized that the linear relation in the loading curve of the blunt tip can be obtained through removing initial L-h curve data during indentation by the blunted part of the tip. When the blunt tip radius is unknown, the initial linear fitting is made within the total curve of the square root of load versus depth and then the tip-blunting correction Δh_b and tip-blunting range h_b are obtained. Again, a second fitting is made after removing the depth range less than h_b from the total loading curve and then Δh_b and h_b are obtained. These procedures are performed iteratively, and ultimately the coefficient K_1 and tip-blunting correction Δh_b in Eq. (8) can be determined when the obtained Δh_b saturates. The values of Δh_b obtained by analyzing loading curves, shown in Fig. 5, agree well with the true input value for the blunt-tip geometry.

B. Relation of W_e/W_{tot} and H/E_r

The linear relation between H/E_r and W_e/W_{total} in Eq. (16) was introduced to derive f from indentation parameters alone. The energy ratio W_e/W_{total} was determined from Eq. (15) with loading and unloading curves, and H was evaluated from contact areas determined from contact profile measurement in FEA. κ was obtained as the slope of linear fit of W_e/W_{total} and H/E_r.

Remarkably, a single κ value could not cover the entire range of W_e/W_{total} and H/E_r in Fig. 6(a), and we thus

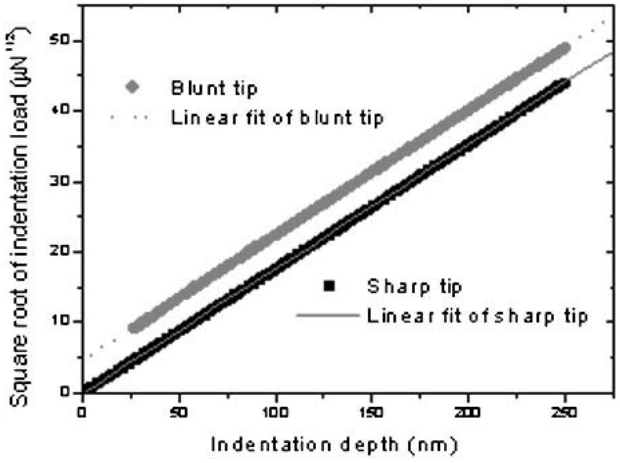

FIG. 4. Square root of applied load ($L^{1/2}$) and depth curves; (◆) and dotted line: blunt tip with 450 nm radius; (■) and solid line: ideally sharp tip.

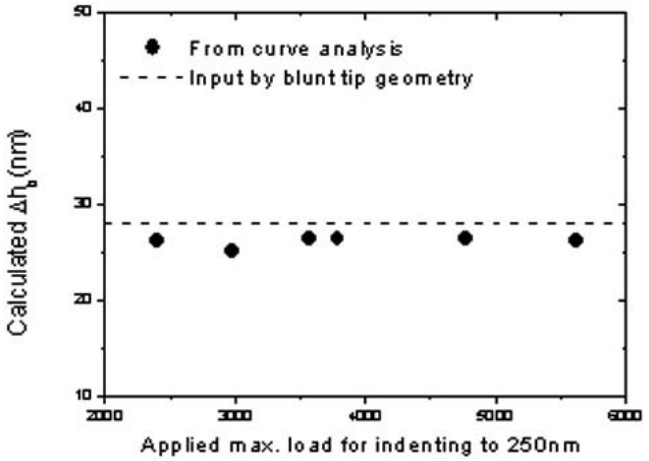

FIG. 5. Δh_b values obtained from loading curve analysis for various materials.

classified κ into 7.30 and 5.17: in the small W_e/W_{total} range ($W_e/W_{total} < 0.15$), κ was 7.30 and in the large W_e/W_{total} range, 5.17. These two κ values were obtained from both of ideally sharp-tip and blunted sharp-tip indentation. In previous research, κ has been reported as a single value of about 5 independent of work-hardening behavior in case of a conical indenter with half-included angle of 70.3° or Berkovich indenter.[9,17–22] However, considerable deviations in their results were also found in the small H/E_r (less than 0.02) and small W_e/W_{total} (less than 0.15) regime. It is notable that a close reanalysis of the results of previous works yields two values of κ with a break point at W_e/W_{total} of 0.15.

This change in κ is related to the competitive pile-up and elastic deflection of materials. When the pile-up is large compared to the elastic deflection, κ is 7.30, but when pile-up is much smaller than elastic deflection, i.e., when sink-in occurs, κ is 5.17 [Figs. 6(b) and 6(c)]. However, FEA results including this study and previous research show that κ is independent of materials properties at least within each regime of $W_e/W_{total} < 0.15$ or $\geqslant 0.15$. Further research is needed in this area.

C. Verification of *f* derived from *L-h* curve and depth independence

The *f* values derived from Eq. (17) using indentation-curve parameters were compared to true *f* values from inspection of contact profiles in FE simulations. Figure 7(a) shows that this curve-analysis method provides more accurate results than the conventional analysis method,[4] especially for ductile materials with large pile-up.

It was also confirmed that *f* is constant regardless of indentation depth in a homogeneous material, as shown in Fig. 7(b). The definition of *f* [Eq. (5)] shows that it depends on the difference between pile-up depth and elastic deflection depth. In other words, the value of *f* is

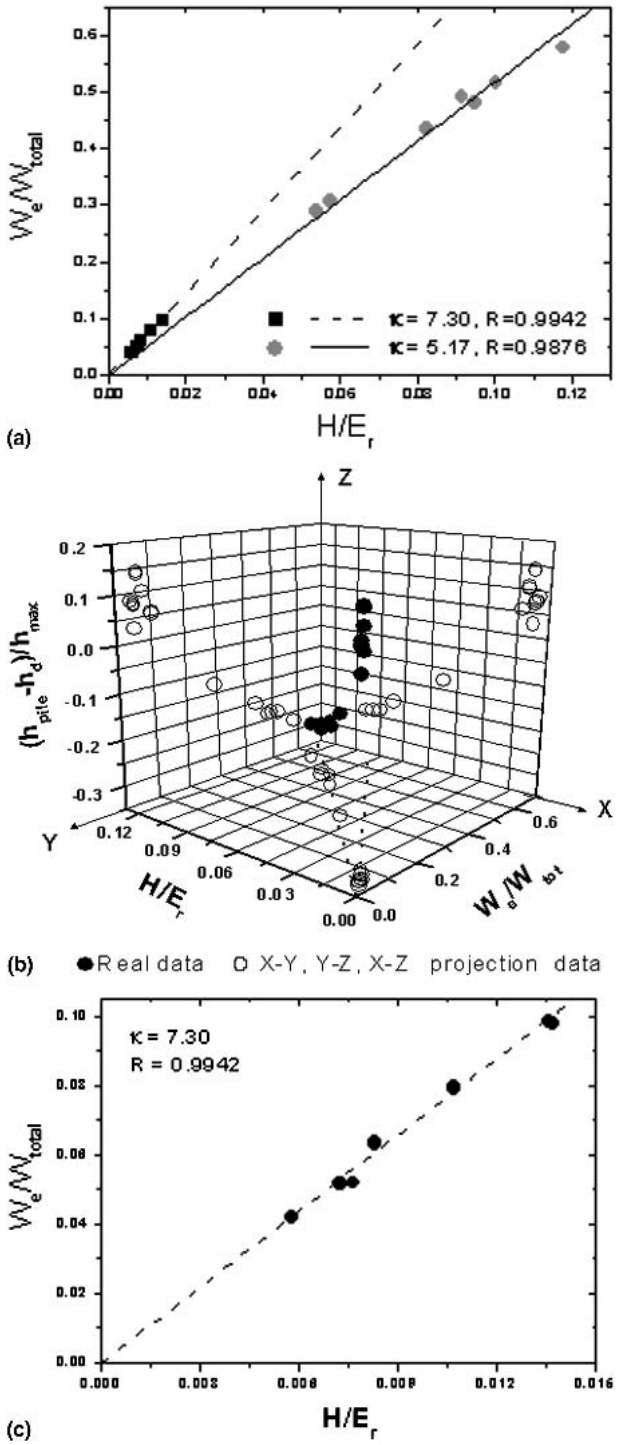

FIG. 6. Interrelation among indentation parameters, pile-up and elastic deflection: (a) relation between W_e/W_{total} and H/E_r in FEA results, (b) competitive pile-up and elastic deflection according to W_e/W_{total} and H/E_r, and (c) enlarged view of $W_e/W_{total} < 0.15$ in (a).

related to both elastic and plastic deformation characteristics of a material, and can be expressed in terms of its elastic and plastic properties. In previous research, the work-hardening exponent, n and the ratio of yield strength to elastic modulus, σ_{ys}/E indenter angle have

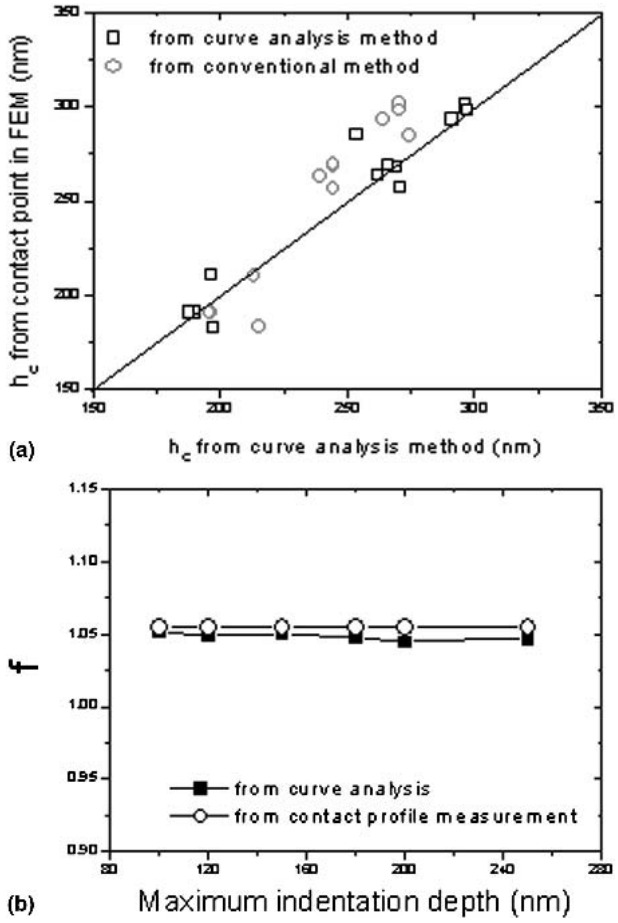

FIG. 7. Results of f verification in FEA: (a) contact depths obtained from the curve-analysis method versus true values from contact profiles measurements, and (b) f independent of maximum indentation depth ($\sigma_{ys}/E_r = 0.003$, $n = 0.187$).

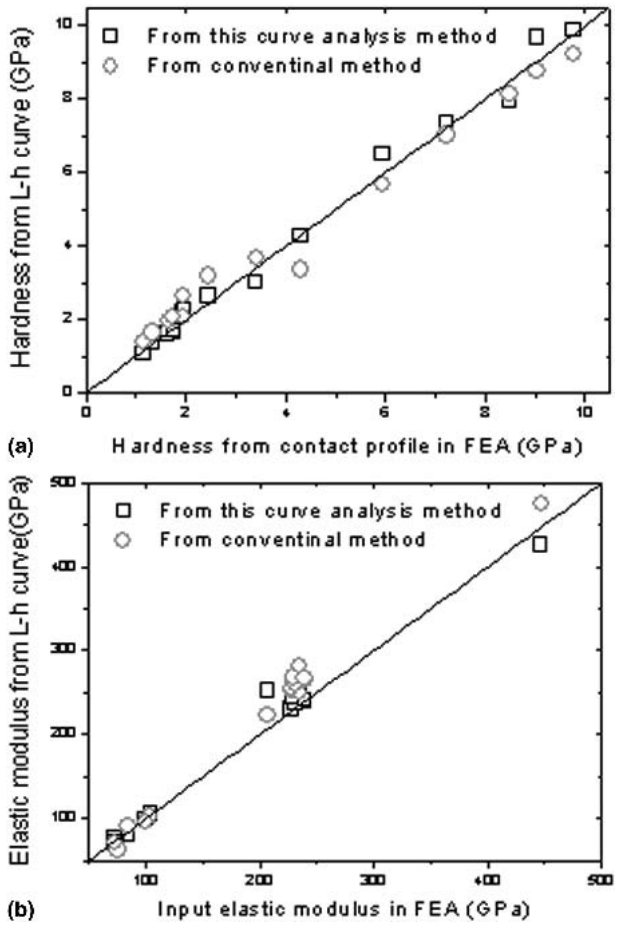

FIG. 8. Hardness and elastic modulus obtained from curve-analysis method versus true values from contact profile measurement in FEA.

been considered as the factors affecting pile-up and sink-in of materials;[7,17,23] as the work-hardening exponent and the ratio of yield strength to elastic modulus decrease, the amount of pile-up increases.[7,17,23] Therefore, it is important to quantify the individual contributions of elastic and plastic parameters to f. We derived the quantitative relation between mechanical properties and the ratio f. A dimensional analysis of FEA results was performed and led to the dimensionless function

$$f = 1.2445(1 - 0.6n)\left(1 - 7.2\,\frac{\sigma_{ys}}{E_r}\right) \quad ,$$

in conical indenter with half-included angle of 70.3°. This function is quite similar to that suggested by Malzbender et al., although their f was defined as $h_c/(h_{max} - h_d)$, not h_c/h_{max} in ideally sharp tip indentation ($\Delta h_b = 0$).[22]

Hardness and elastic modulus were evaluated and are compared with true H values from contact profile measurements and E input for simulation in Fig. 8. In ductile materials with large pile-up, H and E from the curve-analysis method suggested here showed better agreement with the true values than those from the conventional analysis method.[4] This means that this curve-analysis method is effective for contact-area evaluation that takes pile-up/sink-in into account.

D. Applications to nanoindentation tests

Figure 9 shows the ratio f, corrected depth of tip blunting Δh_b, hardness and elastic modulus obtained through the curve-analysis method proposed in this study. At that time, two κ values of 5.17 and 7.30 were applied respectively to the analysis procedures based on their W_e/W_{total} determined from indentation load–depth curves of tested materials. The evaluated Δh_b values of the materials tested [Fig. 9(a)] were found to be similar to the reference value from the tip-calibration procedure, assuming a blunt indenter tip with spherical shape.

Cu and Au film showed large pile-up in AFM observations; on the other hand, glass and fused quartz showed sink-in. Though observations of residual indentations were made, it was difficult to determine f values directly because the profile around the contact impression with

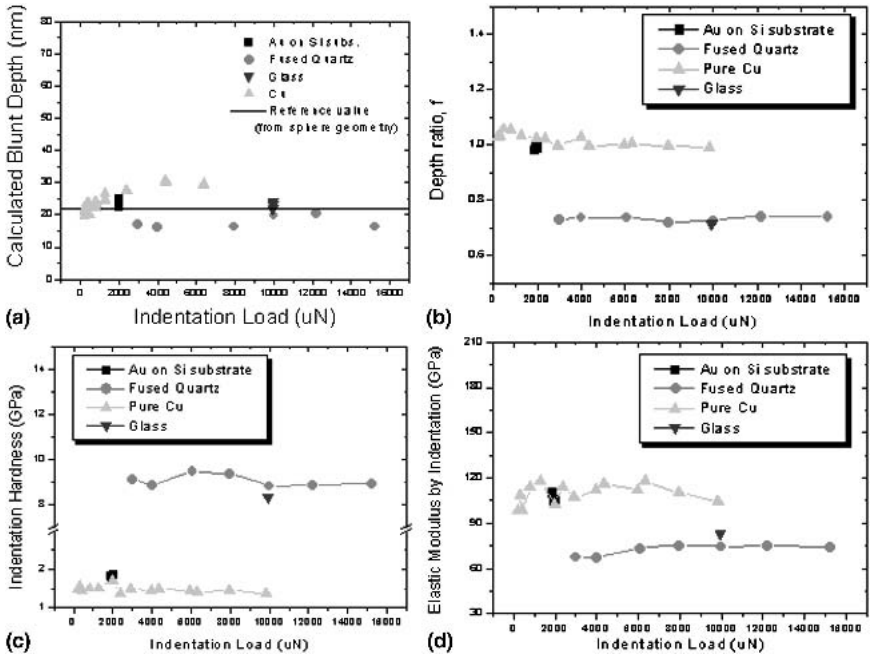

FIG. 9. Nanoindentation results: (a) Δh_b, (b) f, (c) hardness, and (d) elastic modulus of pure Cu, Au film on Si substrate, fused quartz, and glass.

convex or concave shape was not symmetric due to indenter geometry, as shown in Fig. 10. The value of f was evaluated by extracting the square root of the ratio of the real contact area (including pile-up and sink-in) to the triangular cross-sectional indenter area as defined by the indentation corners. We thus assumed that horizontal elastic recovery was negligible. In Cu and fused quartz, the measured f was 1.05 ± 0.02 and 0.76 ± 0.01, respectively, from 1.11 ± 0.04 and 0.58 ± 0.02 of the measured area ratio, and agreed with the f values derived from

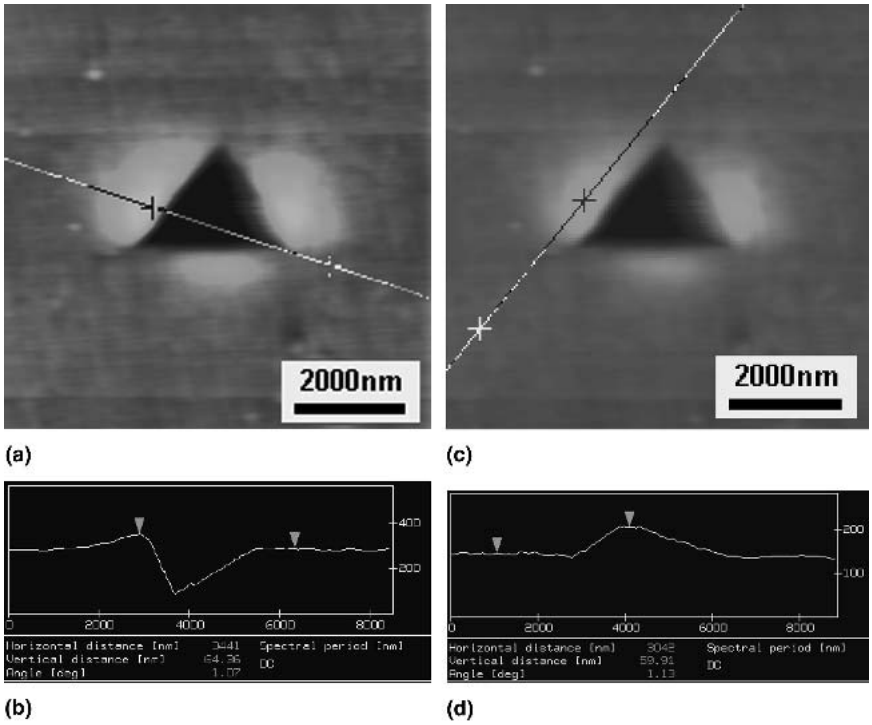

FIG. 10. AFM images of (a, c) pile-up deformation around indentation of pure Cu and (b, d) cross sections with the directions of lines on (a) and (c), respectively [crosses in (a) and (c) correspond to reverse triangles in (b) and (d)].

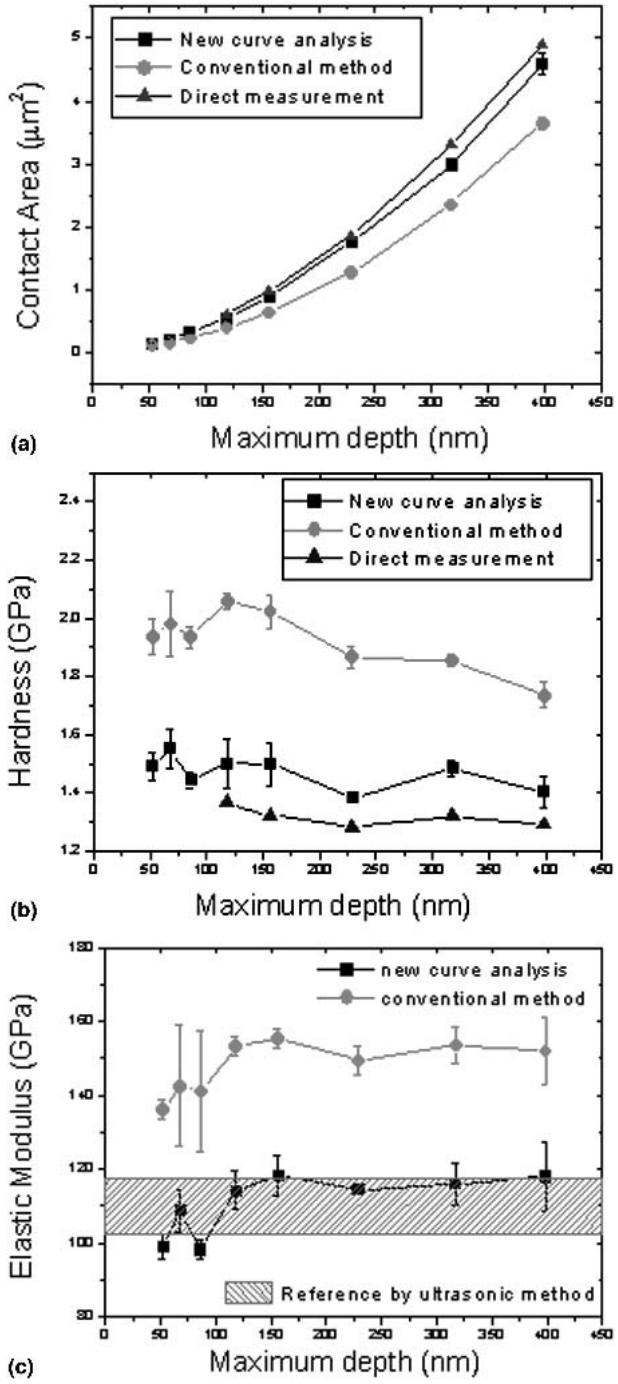

FIG. 11. Comparisons of new curve-analysis method and conventional method for nanoindentation results of pure Cu: (a) contact area, (b) hardness, and (c) elastic modulus.

curve analysis [Fig. 9(b)]. Also, it was confirmed that the f values were almost constant independent of applied load (or maximum indentation depth), as seen in Fig. 9(b).

Hardness and elastic modulus were also evaluated using f, as shown in Figs. 9(c) and 9(d). The elastic modulus values obtained were compared to reference values obtained by an ultrasonic method or micro-beam bending.[24,25] Reference E values for Au on Si, fused quartz, pure Cu and glass were 107.2 ± 4.4, 72, 110 ± 7.6, and 74 GPa, respectively, in good agreement with the values derived from indentations.

In particular, both the new and conventional methods were applied to analyze L-h curves of pure Cu with large pile-up. As reference values, contact areas and hardness were obtained from direct measurements of contact area using AFM, as well as elastic modulus evaluated from ultrasonic method. As expected, contact areas from the conventional method were underestimated, and consequently hardness and elastic modulus overestimated. But the new method could give more accurate results as shown in Fig. 11. Contact area, H and E from the new method agreed well with the reference value.

Consequently, the new indentation curve analysis method could be effectively used for contact area determination considering pile-up and tip-blunting effects. Also, compared to the conventional method, it could provide more accurate results especially for ductile materials with large pile-up.

V. CONCLUSIONS

Indentation contact depth taking into account pile-up, sink-in, and tip-blunting effects was evaluated accurately by the curve-analysis method for both of ideally sharp-tip and blunted sharp-tip indentations. The ratio f of contact depth to maximum depth was defined from contact morphology modeling and was evaluated using only indentation-curve parameters. This ratio was found to be constant regardless of depth and dependent only on indenter geometry and materials properties. On the other hand, the linear relation of W_e/W_{total} and H/E_r was used to derive f and its slope was categorized into two values according to the W_e/W_{total} range. Then hardness and elastic modulus could be evaluated using the contact area calculated from contact depth by an indentation-curve analysis. In particular, this curve-analysis method gave more accurate results than the conventional method for ductile materials with large pile-up.

ACKNOWLEDGMENT

This research was supported by Grant No. 04k1501-01210) from the Center for Nanostructured Materials Technology under the 21st Century Frontier R&D Programs of the Ministry of Science and Technology, Korea.

REFERENCES

1. T.Y. Tsui and G.M. Pharr: Substrate effects on nanoindentation mechanical property measurement of soft films on hard substrates. *J. Mater. Res.* **14,** 292 (1999).
2. N.X. Randall: Direct measurement of residual contact area and

volume during the nanoindentation of coated materials as an alternative method of calculating hardness. *Philos. Mag. A* **82,** 1883 (2002).
3. Y. Choi, W.Y. Choo, J.K. Choi, and D. Kwon: Analysis of mechanical property distribution in multiphase ultra-fine-grained steels by nanoindentation. *Scripta Mater.* **45,** 1401 (2001).
4. W.C. Oliver and G.M. Pharr: An improved technique for determining hardness and elastic modulus using load and displacement sensing indentation experiments. *J. Mater. Res.* **7,** 1564 (1992).
5. J.C. Hay, A. Bolshakov, and G.M. Pharr: A critical examination of the fundamental relations used in the analysis of nanoindentation data. *J. Mater. Res.* **14,** 2296 (1999).
6. G.M. Pharr and A. Bolshakov: Understanding nanoindentation unloading curves. *J. Mater. Res.* **17,** 2660 (2002).
7. A. Bolshakov and G.M. Pharr: Influences of pileup on the measurement of mechanical properties by load and depth-sensing indentation techniques. *J. Mater. Res.* **13,** 1049 (1998).
8. J.L. Hay, W.C. Oliver, A. Bolshakov, and G.M. Pharr: Using the ratio of loading slope and elastic stiffness to predict pileup and constraint factor during indentation, in *Fundamentals of Nanoindentation and Nanotribology*, edited by N.R. Moody, W.W. Gerberich, N. Burnham, and S.P. Baker (Mater. Res. Soc. Symp. Proc. **522,** Warrendale, PA, 1998), p. 101.
9. W.C. Oliver and G.M. Pharr: Measurement of hardness and elastic modulus by instrumented indentation: Advanced in understanding and refinements to methodology. *J. Mater. Res.* **19,** 3 (2004).
10. K.W. McElhaney, J.J. Vlassak, and W.D. Nix: Determination of indenter tip geometry and indentation contact area for depth-sensing indentation experiments. *J. Mater. Res.* **13,** 1300 (1998).
11. J. Mencik and M.V. Swain: Errors associated with depth-sensing microindentation tests. *J. Mater. Res.* **10,** 1491 (1995).
12. Y. Sun, S. Zheng, T. Bell, and J. Smith: Indenter tip radius and load frame compliance calibration using nanoindentation loading curves. *Philos. Mag. Lett.* **79,** 649 (1999).
13. T. Sawa and K. Tanaka: Simplified method for analyzing nanoindentation data and evaluating performance of nanoindentation instruments. *J. Mater. Res.* **16,** 3084 (2001).
14. J.L. Loubet, J.M. Georges, and G. Meille: *Vickers indentation curves of elastoplastic materials*, ASTM STP 889 (ASTM, Philadelphia, PA, 1986), p. 72.
15. S.V. Hainsworth, H.W. Chandler, and T.F. Page: Analysis of nanoindentation load-displacement loading curves. *J. Mater. Res.* **11,** 1987 (1996).
16. R.B. King: Elastic analysis of some punch problems for a layered medium. *Int. J. Solids Struct.* **23,** 1657 (1987).
17. Y. Cheng and Z. Li: Scaling relationships for indentation measurements. *Philos. Mag. A* **82,** 1821 (2002).
18. V. Marx and H. Balke: A critical investigation of the unloading behavior of sharp indentation. *Acta Mater.* **45,** 3791 (1997).
19. A.E. Giannakopoulos and S. Suresh: Determination of elastoplastic properties by instrumented sharp indentation. *Scripta Mater.* **40,** 1191 (1999).
20. Z.H. Xu and D. Rowcliffe: Method to determine the plastic properties of bulk materials by nanoindentation. *Philos. Mag. A* **82,** 1893 (2002).
21. Y-T. Cheng and C-M. Cheng: Relationships between hardness, elastic modulus, and the work of indentation. *Appl. Phys. Lett.* **73,** 614 (1998).
22. J. Malzbender and G. de With: Indentation load-displacement curve, plastic deformation, and energy. *J. Mater. Res.* **17,** 502 (2002).
23. M. Mata, M. Anglada, and J. Alcala: Contact deformation regimes around sharp indentations and the concept of the characteristic strain. *J. Mater. Res.* **17,** 964 (2002).
24. M.A. Meyers and K.K. Chawla: *Mechanical Behavior of Materials* (Prentice Hall, Englewood Cliffs, NJ, 1999), p. 61.
25. D. Son, J-h. Jeong, and D. Kwon: Film-thickness considerations in microcantilever-beam test in measuring mechanical properties of metal thin film. *Thin Solid Films* **437,** 182 (2003).